JOURNAL OF APPLIED PHYSICS **97**, 074303 (2005)

Continuum field model of defect formation in carbon nanotubes

Zhiling Li and Prasad Dharap
Rice University, Houston, Texas 77005

Pradeep Sharma[a)]
University of Houston, Houston, Texas 77204

Satish Nagarajaiah and Boris I. Yakobson
Rice University, Houston, Texas 77005

(Received 29 June 2004; accepted 24 January 2005; published online 21 March 2005)

While considerable efforts in the form of (numerical) atomistic simulations have been expended to understand the mechanics of defect formation under applied strain, analogous analytical efforts have been rather few. In this work, based on the physics at the nanoscale, defect nucleation in single-walled carbon nanotubes is studied using both classical continuum field theory as well as gauge field theory of defects. Despite the inherent continuum assumption in our models, reasonably close qualitative and quantitative agreement with existing atomistic simulations is obtained. The latter lends credence to the belief that continuum formulations, with correct incorporation of the relevant physics, can be a powerful and yet simple tool for exploring nanoscale phenomena in carbon nanotubes. The results are more sensitive to chirality than to the size of the nanotubes. © *2005 American Institute of Physics*. [DOI: 10.1063/1.1870102]

I. INTRODUCTION AND MOTIVATION

The study of defects in carbon nanotubes (CNTs) is rapidly acquiring considerable importance. Various types of defects that form in CNTs severely impact their optoelectronic properties and mechanical behavior.[1] As often expressed in previous work,[2] defect formations in CNTs are also responsible for the so-called "nanoplasticity" and "brittle-ductile" transition. It hardly seems unreasonable to contend that future structure, systems, and devices made from CNTs will be highly sensitive to defects. Defect generation and growth have been observed during plastic deformation and fracture of CNTs. Topological defects are also necessary to form junctions and thus are ubiquitous in electronic device applications, among others. For example, a two-terminal heterojunction formed by two nanotubes, one semiconducting and the other metallic, can function like a rectifying diode.[3]

Considering the importance of this topic from both fundamental and technological perspectives several works that address this issue theoretically have appeared in recent times. The foundational work in this, from a theoretical perspective, is found in Refs. 2 and 4–6, where, using massive atomistic simulations, the formation of a 5-7-7-5 defect in single-walled CNTs (SWCNTs) under uniaxial tension is discussed. The aforementioned atomistic simulations have provided profound insights into the microscopic mechanics of defects under applied strain. However, computational expense often precludes the extension of atomistic simulations to very large systems. Further, and perhaps more important, often a mapping of atomistic numerical results to simpler analytical models is highly desirable which captures the essence of the physics of the numerical results through appropriate parametrization in terms of well-defined material constants (e.g., Burgers vector, elastic moduli, and so forth). In this work, we present a continuum field interpretation of this phenomenon which incorporates the physics of the defect nucleation process in SWCNTs. In addition, we also attempt a semianalytical solution based on the gauge field theory of defects, which (as has been demonstrated for simple defects) is capable of removing the singularities that plague the classical continuum formulation of defects. Our two solutions, one based on classical continuum mechanics and the other on gauge field theory, are compared with each other. As will be noted in due course, both provide reasonable answers with only slight numerical differences although the gauge field approach is far more physical and less *ad hoc*. Our analytical and semianalytical expressions, while approximate, provide a clear basis for both a stand-alone interpretation as well as a complement to already published atomistic results and can be extended to the realistic system of large scale.

Consider the often-discussed case of a SWCNT subjected to a uniaxial strain along its longitudinal direction. Below a critical strain, CNTs simply stretch elastically. However, beyond that critical strain, CNTs prefer to lower the accumulated strain energy by the rotation of one of the C–C bonds rather than stretching elastically.[2,5–8] This accommodation mechanism (i.e., rotation of the C–C bond) results in the formation of a pentagon pair and a heptagon pair. This is often termed as the Stone–Wales (SW) defect. Atomistic simulations indicate that the SW defect becomes energetically favored at ~6% strain in an armchair nanotube,[2,5–7] whereas this defect is unfavorable up to a very high strain value (over 12%) in a zigzag nanotube.[6,7]

The outline of this article is as follows. In Sec. II, we discuss some relevant background and review published results in this area. Our continuum field and gauge theory based formulations for the SW defect formation in graphene sheets and nanotubes are presented in Sec. III. We discuss

[a)]Electronic mail: psharma@uh.edu

TABLE I. Predicted formation energies and critical strains of graphene sheet and CNTs based on atomic simulations.

Reference	Formation energy at zero-strain graphene sheet/armchair/zigzag (eV)	Critical strain % graphene sheet/armchair/zigzag
Zhao *et al.*[6]	~5.0/~4.0(5,5)/~4.0(9,0)	6.0/7.5/12.0
Nardelli *et al.*[5]	~2.5/~2.0(5,5)/-	6.0/5.2/-[a]
Yakobson *et al.*[4]	⋯	40[b]
Brabec *et al.*[8]	2.35 (5-7-7-5)	⋯
Nardelli *et al.*[2]	~2.0 (5-7-8-7-5)	⋯
Zhou and Shi[9]	-/~5.3(10,10)/~4.6(20,0)	⋯
Zhang *et al.*[7]	-/~4.0(6,6)/~4.0(12,0)	-/6.0(6,6)/12(12,0)

[a]Simulations are carried at 1800 K.
[b]Simulations are carried at 50 K.

our results in Sec. IV and compare with existing atomistic simulations. We finally conclude with a summary in Sec. V.

II. BACKGROUND AND REVIEW OF EXISTING WORK

Several works have provided insights into this particular problem. Zhao *et al.*,[6] based on tight-binding calculations, reported that the defect becomes energetically favorable at strains of the order of 7–8% in an (5, 5) armchair CNT and at about 10.5% strains for a (9, 0) zigzag CNT. Corresponding defect nucleation strain from *ab initio* calculations for an (5, 5) armchair CNT is about 6%. Nardelli *et al.*[5] have also reported that the defect structure becomes energetically favorable after about 5.2% strains in a (5,5) tube. Nardelli *et al.*[5] carried out simulation using a classical many-body Tersoff–Brenner potential. Critical strain for an armchair CNT (6, 6) is ~6% and for a zigzag tube (12, 0) is ~12% as reported by Zhang *et al.*[7] using tight-binding molecular dynamics calculations. However, it is interesting to note some discrepancies in published values for a (5, 5) CNT as well as graphene sheet.[5,6] Zhao *et al.*[6] reported the formation energy for a graphene sheet at zero strain to be about ~6 eV while that for (5, 5) tubes is ~4 eV. On the other hand, Nardelli *et al.*[5] reported the formation energy for a graphene sheet at zero strain to be about ~2.5 eV while that for (5, 5) CNTs is ~2 eV. Yakobson *et al.*[4] mentioned that preliminary molecular dynamics results using the many-body Tersoff–Brenner potential (at $T=50$ K) show a tube stretched by almost 40% with no damage to its graphitic arrangements. It should be noted that Nardelli *et al.*[5] carried out simulations at 1800 K so that the activation barrier in order to rotate the C–C bond can be overcome. At room temperature, the activation energy barrier for C–C bond rotation is significant and thus the nanotube continues to deform elastically without the formation of any defects. Hence, at room temperature, the CNTs are very stable in their hexagonal equilibrium configuration.[4,5]

In the present work, we solely address the formation energy (and not the activation energy) for a SW defect. For easy reference, existing results on defect formation are summarized in Table I.

III. FORMULATION

The key to our approach is the casting of the SW defect into equivalent topological defects in crystalline structures that are relatively well understood and analyzed; namely, dislocations and disclinations. Such an exercise enables the use of several readily available results for latter defects. Figure 1 shows the uniaxial stretching of a CNT and formation of a SW defect corresponding to both an armchair and a zigzag configuration. Note the difference in the orientation of the C–C bond, the rotation of which results in a SW defect. In this study, nucleation of a SW defect in a graphene sheet is considered in configurations similar to ones shown in Fig. 1, ignoring the curvature effects due to rolling of a graphene sheet to form a CNT.

In a subsequent analysis of the graphene sheet, plane stress conditions are considered to be operative and out-of-plane buckling is ignored. A uniaxial strain ϵ^{∞} is applied at infinity in the x direction on the graphene sheet (Fig. 1). In a rectangular coordinate system, the stresses are well known to be:[10] $\sigma_{xx}^{\infty}=E\epsilon^{\infty}/(1-\nu^2)$, $\sigma_{yy}^{\infty}=\nu E\epsilon^{\infty}/(1-\nu^2)$, $\sigma_{xy}^{\infty}=0$, where ν is Poisson's ratio, and E is Young's modulus of the graphene

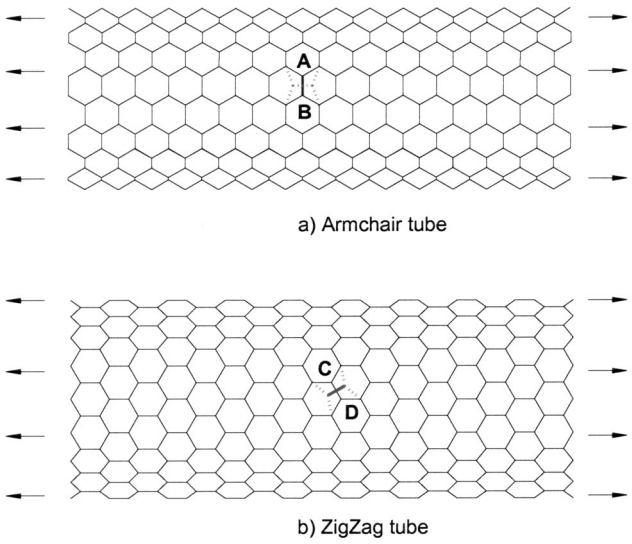

FIG. 1. Uniaxial stretching and formation of a SW defect in a CNT: (a) An armchair carbon nanotube and (b) a zigzag carbon nanotube. (This figure is adapted from Zhao *et al.*, see Ref. 6).

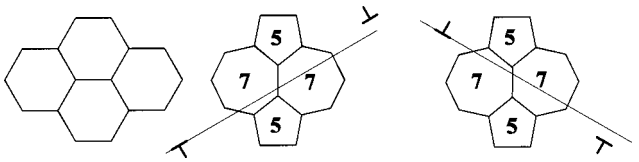

FIG. 2. Rotation of C–C band in the SW defect can be represented by four disclinations (5-7-7-5), and the four disclinations form an edge dislocation dipole.

sheet. Our main premise is that the rotation of the C–C bond for the SW defect in a graphene sheet can be treated as the formation of two pairs of heptagon/pentagon (7/5) disclinations. This is shown schematically in Fig. 2.

In Sec. III A, we start with the discussion of the SW defect formation in a graphene sheet. The formation energy and the critical strain formulae using classical theory as well as gauge theory are discussed. Subsequently, in Sec. III B, we will consider defect nucleation in CNTs by taking into account curvature effects due to the rolling of a graphene sheet.

A. Graphene sheet

From a purely topological point of view [see for example, Nelson (Ref. 11)], a pair of heptagon/pentagon disclination pair can be grouped to form an edge dislocation, and an edge dislocation pair will form a dipole, as shown in Fig. 2. The corresponding Burgers vector can be approximately calculated as: $\mathbf{b}_k \cong \mathbf{z} \times \boldsymbol{\delta}_k$, where $\mathbf{z}$ is the normal direction of the graphene sheet and $\boldsymbol{\delta}_k$ is the vector from the center of pentagon disclination to the center of heptagon disclination (the accurate value of Burgers vector of each 5/7 defect is equal to the lattice constant of the graphene sheet). Thus, the rotation of C–C bond in a graphene sheet can be conceived of as the nucleation of an edge dislocation dipole. Due to the D_{2h} symmetry of the SW defect, it requires that the representation of a SW defect be one-half of the sum of that produced by the representing dipoles,[12,13] as shown in Fig. 2.

Now, we employ a simple energy based criterion to estimate the strain at which the SW defect (or in our approach, an edge dislocation dipole) is nucleated. A similar approach is often also followed in thin films; we can express the total energy of the graphene sheet as

$$W = W_E + W_D + W_I, \tag{1}$$

where W_E is the stored elastic strain energy of the graphene sheet in absence of a defect (induced by the stress due to applied strain at infinity, henceforth called the applied stress field), W_D is the self-energy of the nucleated edge dislocation dipole (that simulates the SW defect), and W_I is the interaction energy between the applied stresses and the dislocation dipole. The change in the energy of the graphene sheet relative to its defect-free state can be written as

$$\Delta W = W_D + W_I. \tag{2}$$

Clearly, defect nucleation then becomes favorable if this change in energy is zero or less.

We begin by first employing classical continuum method. In this approach, the self-energy for the edge dislocation pair can be written as[14]

$$W_D = \frac{\mu b^2 h}{2\pi(1-\nu)}\left(\ln\frac{\alpha r}{b} - \gamma\right), \tag{3}$$

where α is usually taken to be 3 as suggested in Ref. 13, μ is the shear modulus, r is the distance between centers of the two edge dislocations, and h is the thickness of the graphene sheet. γ is given as $1-2\nu/4(1-\nu)$. An implicit assumption of Eq. (3), is that the two-edge dislocations are separated such that the distance r is greater than the cutoff radius of the edge dislocation. This is somewhat problematic since, in our case, r is less than the Burgers vector. So, Eq. (3) can only be an approximation of the self-energy of the dislocation dipole. As is well known [and obvious from Eq. (3)], the solution of dislocations by classical continuum mechanics contains singularities at the dislocation line, which somewhat contradict its application within the dislocation core region or for very short dipole separations. This is unfortunate since, as mentioned earlier, in the present case the two-edge dislocations are indeed located very close to each other. There are several nonstandard continuum models of dislocations, such as the nonlocal continuum model,[15,16] strain gradient elasticity,[17,18] quasi-continuum model,[19] and gauge dislocation theory.[20–22] For reasons mentioned earlier in the introduction, we prefer the gauge theory. Dislocations and other topological defects, in this theory, are seen to arise naturally via simply symmetry conditions and obviate the need for *ad hoc* postulates. In addition, the divergence of the stress fields and the energy is removed. Further, other methods, such as the quasi continuum method (which can also remove the singularities),[19] appear to exhibit oscillations in its stress solutions, which can be rather unphysical. So, those methods are not adopted here. In contrast, the results for edge dislocation given by the gauge theory not only converge at the dislocation line, but also match the classical continuum solution at the far field.[21] Unfortunately, the solution based on the gauge field theory is only available for a *single*-edge dislocation. We herein present a gauge theory solution for the interaction energy between two-edge dislocations, which is necessary for the present formulation.

To arrive at a gauge solution for the present problem under consideration, we begin by employing the stress and energy function for a single-edge dislocation derived by Lazar[21] and the broad procedure employed in Refs. 20 and 22. The total energy of the dislocation dipole can then be expressed as:[20,22]

$$W_D^{\text{gauge}} = \int_\nu (W_e + sW_p)\, d\nu,$$

$$W_e = \frac{1}{2}[\lambda(\varepsilon_{ii})^2 + 2\mu\varepsilon_{ij}\varepsilon_{ij}], \tag{4}$$

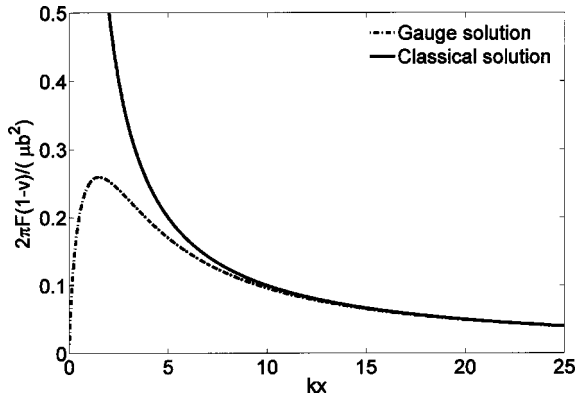

FIG. 3. The interaction force F between an edge dislocation dipole as a function of separation distance R of the dislocation dipole. Note that both F and R are expressed in dimensionless units. Our gauge solution is compared with the classical one.

$$W_p = \frac{1}{2}F_{ij}^m F_{ij}^m \text{ and } F_{ij}^m = \phi_{mj,i} - \phi_{mi,j},$$

where s is a coupling constant, ϕ represent the so-called gauge fields, λ is the Lamé constant, ε_{ij} is the gauge version of strain of the graphene sheet due to the edge dislocation dipole, and F_{ij}^m is the dislocation density of an edge dislocation. For the edge dislocation dipole, by considering the center of the one-edge dislocation to be origin and the other at $\mathbf{R}=(R_x,R_y)$, the strains and dislocation density of an edge dislocation dipole at point $\boldsymbol{\rho}$ can be obtained by superposition:

$$\begin{aligned}\varepsilon_{ij} &= \varepsilon_{ij}(\kappa,\rho) + \varepsilon_{ij}(\kappa,\rho'),\\ F_{ij}^m &= F_{ij}^m(\kappa,\boldsymbol{\rho}) + F_{ij}^m(\kappa,\boldsymbol{\rho}'),\end{aligned} \tag{5}$$

where $\kappa=\sqrt{2\mu/s}$ and $\boldsymbol{\rho}'=\boldsymbol{\rho}-\mathbf{R}$. Further details of our gauge solution to the interaction energy between two-edge dislocations will be reported elsewhere. To illustrate our gauge solution, we have plotted the numerically calculated force between the two dislocations and compared it with the classical solution in Fig. 3. It can be observed that, in the gauge solution, the interaction force between an edge dislocation dipole is zero when R is equal to zero (which conforms to intuition) in contrast with the infinite interaction force given by classical solution.

Finally, to complete our model, we need the interaction energy between the applied stress field and the dislocation dipole that represents the SW dipole. From dislocation theory, we can evaluate it by

$$W_I = \int_\nu \sigma_{ij}^\infty \varepsilon_{ij} d\nu, \tag{6}$$

where σ_{ij}^∞ is the applied stress field due to uniaxial strain ε^∞, and ε_{ij} is the strain field due to dislocation dipole. Interaction energy between the applied stress field and the dislocations is equal to the work done by stress in deforming the system from its original shape, which can be described by the Peach–Koehler formula:[23,12,13,24]

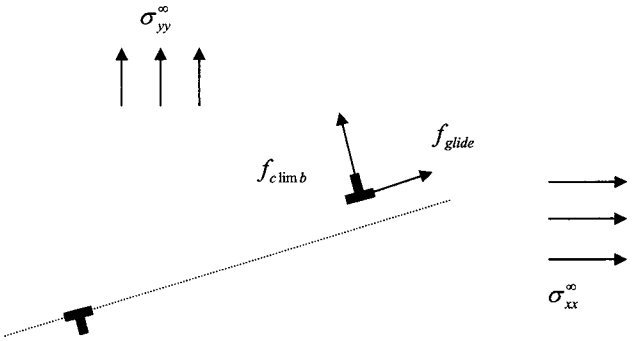

FIG. 4. Peach–Koehler force due to external stresses.

$$f_k = -\varepsilon_{ijk} n_i \sigma_{jm}^\infty b_m, \tag{7}$$

where ε_{ijk} is the Levi–Civita permutation symbol, σ_{jm}^∞ is the external stress, n_i is dislocation line direction, and b_m is the Burger vector in the m direction. With the D_{2h} symmetry of the SW defect, the Peach–Koehler force glide force and climb force (see Fig. 4) can be obtained:[12,13]

$$\begin{aligned}f_{\text{glide}} &= \mu\varepsilon^\infty bh \sin\left(2\chi + \frac{\pi}{6}\right),\\ f_{\text{climb}} &= \mu\varepsilon^\infty bh\left(\frac{1+\nu}{1-\nu} - \cos\left(2\chi + \frac{\pi}{6}\right)\right),\end{aligned} \tag{8}$$

where χ is the chiral angle of the graphene sheet corresponding to the nanotube. From the changes in the topology, the SW defect is equivalent to either of the two dipoles resulting from an $a/2$ slip in the hexagonal lattice,[25] where a is the lattice constant of the graphene sheet/nanotube. Also, there exists a $a/2\sqrt{3}$ climb between the two dipoles, as shown in Fig. 4. Then, the energy due to the externally applied stress can be expressed as:

$$\begin{aligned}W_I &= f_{\text{glide}}\frac{a}{2} + f_{\text{climb}}\frac{a}{2\sqrt{3}}\\ &= \frac{\mu\varepsilon^\infty bah}{2}\left[\sin\left(2\chi + \frac{\pi}{6}\right)\right.\\ &\quad \left. + \frac{1}{\sqrt{3}}\left(\frac{1+\nu}{1-\nu} - \cos\left(2\chi + \frac{\pi}{6}\right)\right)\right].\end{aligned} \tag{9}$$

Thus, the defect becomes energetically favorable when $\Delta W<0$. At this point, the system lowers its energy by formation of a defect rather than stretching elastically.

Finally, the critical strain predicted based on classical elasticity is obtained by

$$\varepsilon_{\text{crit}} = \frac{b}{\pi(1-\nu)a\left[\sin\left(2\chi+\frac{\pi}{6}\right)+\frac{1}{\sqrt{3}}\left(\frac{1+\nu}{1-\nu}-\cos\left(2\chi+\frac{\pi}{6}\right)\right)\right]}\left(\ln\frac{\alpha r}{b}-\gamma\right). \tag{10a}$$

If the self-energy is calculated using the gauge theory, the critical strain for the defect to be favorable can be obtained as:

$$\varepsilon_{\text{crit}} = \frac{W_D^{\text{gauge}}}{\frac{\mu\varepsilon^{\infty}bah}{2}\left[\sin\left(2\chi+\frac{\pi}{6}\right)+\frac{1}{\sqrt{3}}\left(\frac{1+\nu}{1-\nu}-\cos\left(2\chi+\frac{\pi}{6}\right)\right)\right]}, \tag{10b}$$

It can be observed from Eq. (10) that the critical strain for nucleation of the SW defect predicted by both the classical solution and gauge theory is independent of Young's modulus of the graphene sheet. We note though that the critical strain does depend on the Poisson's ratio of the graphene sheet and angle between the applied stress and Burgers vector.

B. Carbon nanotube

We now turn our attention to the CNT. As we alluded to earlier, the nanotube containing a defect can be viewed appropriately as a rolled-up graphene sheet. The energy of the nanotube is

$$W = W_E + W_D + W_I + W_{b1} + W_{b2}, \tag{11}$$

where the first three terms on the right-hand side of Eq. (11) are the same as that of the graphene sheet in Eq. (1), W_{b1} is the energy due to bending the graphene sheet in its defect-free state to form the nanotube. This energy can be calculated as $W_{b1}=Eh^3/24\,\Omega/R_N^2$, where Ω is the atomic volume, and R_N is the radius of the nanotube. W_{b2} is the change in the energy due to a dislocation dipole in the nanotube when compared to the graphene sheet.

As pointed out by Nelson,[11] the dislocation dipole in a graphene sheet is equivalent to four disclinations. The formation energy of four disclinations in a cylindrical curved surface can be solved by the method presented by Lenz and Nelson.[25] But, as shown by atomistic simulations,[5–8] the critical strain and formation energy of the nanotube are only weakly dependent on the diameter of the nanotube. So, some approximations are made in this article and a much more simple approach is adopted here. The difference in the energy of a dislocation dipole in the graphene sheet and the nanotube is due to the curvature of the nanotube. The dislocation dipole will cause out-of-plane buckling in the graphene sheet as well as in the nanotube. Only a small region around the SW defect will buckle out of plane and the rest will remain flat in case of the graphene sheet and on the surface of cylinder in case of the nanotube. A change in energy due to the SW defect is assumed to be limited to the small region around the SW defect, which is denoted as S_b. Assuming the curvature of the graphene sheet at point $\boldsymbol{\rho}$ due to the buckling of the dipole to be $\kappa_d(\boldsymbol{\rho})$ and the curvature of the nanotube be $\kappa_0(\boldsymbol{\rho})$, the buckling energy of the dipole in the nanotube can be approximated by:

$$\begin{aligned} W_{\text{bulking}} &= \int_{S_b}\frac{1}{2}c(\kappa_d(\boldsymbol{\rho})-\kappa_0(\boldsymbol{\rho}))^2 ds \\ &= \int_{S_b}\frac{1}{2}c\kappa_d^2(\boldsymbol{\rho})ds + \int_{S_b}\frac{1}{2}c\kappa_0^2(\boldsymbol{\rho})ds \\ &\quad - \int_{S_b} c\kappa_0(\boldsymbol{\rho})\kappa_d(\boldsymbol{\rho})ds, \end{aligned} \tag{12}$$

where c is the elastic bending constant (with the units of energy). For out-of-plane curvature, the first term on the right-hand side of Eq. (12) is the buckling energy of the dislocation dipole in the graphene sheet. The second term on the right-hand side of Eq. (12) is the energy in the region S_b due to bending the graphene sheet into the nanotube. The third term on the right-hand side of Eq. (12), $W_{b2}=-\int_{S_b}c\kappa_0(\boldsymbol{\rho})\kappa_d(\boldsymbol{\rho})ds=-\int_{S_b}c/d\kappa_d(\boldsymbol{\rho})ds$, is the couple energy due to the curvature of the nanotube and dislocation buckling, where d is the diameter of the nanotube. With the assumption that k_0 and k_d are scalar, the chiral angle χ dependent term for the bending part is ignored in this analysis. This term will be used to approximate the difference in the energy of a dislocation dipole in the graphene sheet and the nanotube. The mean curvature κ_d due to the dislocation dipole in a graphene sheet is assumed to be 0.04 (1/Å) in this article. Using the same energy-based defect nucleation criterion as for the graphene sheet, we can write

$$\Delta W = W_D + W_I + W_{b2}. \tag{13}$$

The critical strain of the nanotube for defect to be energetically favorable is obtained (the classical continuum solution):

$$\varepsilon_{\text{crit}} = \frac{b}{\pi(1-\nu)a\left[\sin\left(2\chi+\frac{\pi}{6}\right)+\frac{1}{\sqrt{3}}\left(\frac{1+\nu}{1-\nu}-\cos\left(2\chi+\frac{\pi}{6}\right)\right)\right]}\left(\ln\frac{\alpha r}{b}-\gamma\right)$$

$$-\frac{1}{\frac{\mu\varepsilon^{\infty}bah}{2}\left[\sin\left(2\chi+\frac{\pi}{6}\right)+\frac{1}{\sqrt{3}}\left(\frac{1+\nu}{1-\nu}-\cos\left(2\chi+\frac{\pi}{6}\right)\right)\right]}\int_s \frac{c}{d}\kappa_0(\boldsymbol{\rho})ds, \tag{14a}$$

Correspondingly, the critical strain of the nanotube predicted using the gauge theory is obtained as

$$\varepsilon_{\text{crit}} = \frac{W_D^{\text{gauge}}}{\frac{\mu\varepsilon^{\infty}bah}{2}\left[\sin\left(2\chi+\frac{\pi}{6}\right)+\frac{1}{\sqrt{3}}\left(\frac{1+\nu}{1-\nu}-\cos\left(2\chi+\frac{\pi}{6}\right)\right)\right]}$$

$$-\frac{1}{\frac{\mu\varepsilon^{\infty}bah}{2}\left[\sin\left(2\chi+\frac{\pi}{6}\right)+\frac{1}{\sqrt{3}}\left(\frac{1+\nu}{1-\nu}-\cos\left(2\chi+\frac{\pi}{6}\right)\right)\right]}\int_s \frac{c}{d}\kappa_0(\boldsymbol{\rho})ds. \tag{14b}$$

IV. RESULTS, DISCUSSION, AND COMPARISON WITH EXISTING ATOMISTIC SIMULATIONS

In this section, formation energy and critical strain—for the nucleation of an edge dislocation dipole for the graphene sheet and CNTs for both an armchair and zigzag configuration—are calculated and compared with the existing atomistic simulation results. Sensitivity of the formation energy at zero strain and critical strain for the nucleation of an edge dislocation dipole to the chirality of the nanotube as well as to the size of the CNT is discussed. We have used the following numerical values in our calculations:[26] Young's modulus E of the graphene sheet is 1.08 TPa, Poisson ratio ν equals 0.19, the C–C bond length is 1.4 Å, the lattice constant of the graphene sheet a is 2.43 Å, and the thickness of the graphene sheet h is 3.35 Å. The out-of-plane bending elastic constant c is 1.02 eV. Finally, in the gauge solution, an inverse characteristic length scale $\kappa = 1/(0.40a)$ is adopted as proposed by Altan and Aifantis.[27]

A. Armchair carbon nanotube and corresponding graphene sheet

First results for an armchair nanotube and the graphene sheet with a configuration corresponding to an armchair CNT are discussed. The graphene sheet is rolled to form a CNT and, depending upon the rolling direction, CNTs with different chiral angles are formed, e.g., an armchair CNT with a chiral angle 30° and a zigzag CNT with angle 0°. All other nanotubes have chiral angles between 0° and 30°. While a graphene sheet *per se* does not have an "armchair" or "zigzag" configuration, however, when formed by the unrolling of a nanotube of a specific chirality, the angle at which the applied strain acts will be different depending upon the chirality. We term such a graphene sheet as one "corresponding" to the specified chirality, i.e., in the present case, an armchair sheet.

For the graphene sheet that corresponds to an unrolled armchair nanotube, the chiral angle χ is 30°. Formation energy of the edge dislocation dipole in the graphene sheet varies with the uniaxial strain as shown in Fig. 5. It can be observed that the formation energy of the edge dislocation dipole decreases when uniaxial strain in the x direction increases. The critical strain at which the defect becomes energetically favorable is the strain corresponding to zero-formation energy in Fig. 5 and can be calculated using Eq. (10). As shown in Fig. 5, the gauge solution yields the critical strain for an (5,5) armchair CNT as 6.24% and for corresponding graphene sheet as 6.50%. This matches well with the results given in the literature.[2,4–6] The critical strain for an armchair CNT, as predicted by the classical elasticity solution, is 7.61% and that for corresponding graphene sheet is 7.30%, which is also close to the result given in literature.[2,4–6] It can be observed that the formation energy of

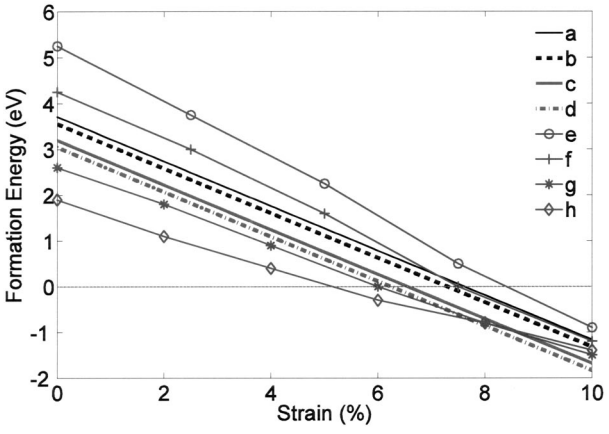

FIG. 5. Formation energy of an edge dislocation dipole as a function of uniaxial strain for an armchair CNT: (a) Graphene sheet present work: Classical continuum solution; (b) (5,5) armchair CNT present work: Classical continuum solution; (c) Graphene sheet present work: Gauge field theory; (d) (5,5) armchair CNT present work: Gauge field theory; (e) Graphene sheet atomistic results (see Ref. 6); (f) (5,5) armchair CNT atomistic results (see Ref. 6); (g) Graphene sheet atomistic results (see Ref. 5), and (h) (5,5) armchair CNT atomistic results (see Ref. 5).

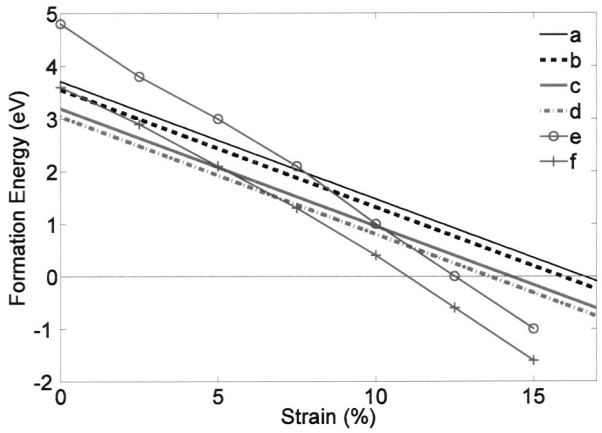

FIG. 6. Formation energy of an edge dislocation dipole as a function of uniaxial strain for a zigzag CNT: (a) Graphene sheet present work: Classical continuum solution; (b) (9,0) zigzag CNT present work: Classical continuum solution; (c) Graphene sheet present work: Gauge field theory; (d) (9,0) zigzag CNT present work: Gauge field theory; (e) Graphene sheet atomistic results (see Ref. 6); and (f) (9,0) zigzag CNT atomistic results (see Ref. 6).

the CNT at zero strain is less than that of the graphene sheet as shown in Fig. 5. Also, critical strain for nucleation of an edge dislocation dipole in a CNT is less than that of for a graphene sheet. The differences in the formation energy at zero strain and in critical strain for the nucleation of an edge dislocation dipole can be attributed to the additional bending energy in a CNT due to the rolling of a graphene sheet to form a CNT. Atomistic simulation results are also plotted in Fig. 5. Clearly, while both classical and gauge solutions are reasonable, the latter gives results closest to the existing atomistic simulation results.[2,6]

B. Zigzag carbon nanotube and corresponding graphene sheet

The nucleation of an edge dislocation dipole is studied in a zigzag CNT and the results are compared with the corresponding graphene sheet, armchair CNT, as well as existing atomistic simulations of other researchers.

For the graphene sheet corresponding to a zigzag configuration, the chiral angle χ is 0°. Variation of the formation energy of the edge dislocation dipole in the graphene sheet with the uniaxial strain is shown in Fig. 6. We find, based on our models, the critical strain for a (9,0) nanotube to be 15.90% and the critical strain for the corresponding graphene sheet to be 16.58% using classical continuum mechanics. Using the gauge theory, the critical strains obtained are, for a (9,0) nanotube, 13.61% and corresponding graphene sheet, 14.29%. It appears that this defect is unfavorable up to a very high strain value ($\sim$14%) in a zigzag nanotube as compared to $\sim$6% strain in an armchair nanotube. In a zigzag tube, the C–C bond, which rotates to form an edge dislocation dipole forms a 60° angle with the tube axis, as compared to 90° in case of an armchair tube and thus cannot effectively release the stress.[6]

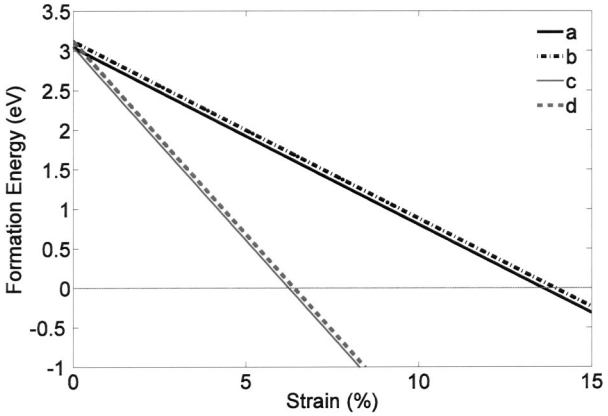

FIG. 7. Gauge field theory solution of formation energy of an edge dislocation dipole as a function of uniaxial strain for CNTs with different diameters and different chiralities: (a) (9,0) Zigzag CNT; (b) (18,0) zigzag CNT; (c) (5,5) armchair CNT; and (d) (10,10) armchair CNT.

C. Sensitivity to size and chirality of carbon nanotube

Formation energies as a function of uniaxial strain in the x direction for different diameters and chiralities of nanotubes are plotted in Fig. 7. It can be observed that the formation energy of the nanotube with the same chirality is less for a smaller diameter of nanotubes. The same observation can be made about the critical strain for the nucleation of an edge dislocation dipole. The lower formation energy and lower critical strain are due to increased bending energy in CNTs with smaller diameters. Note that the critical strain for nucleation of a dislocation dipole in CNTs depends on the diameter, as well as the chirality of the carbon nanotube, though a change in critical strain for nanotubes with different diameters is small as compared to change in critical strain for nanotubes with different chiralities.

The critical strain for a CNT, whether it is an armchair or a zigzag CNT, is smaller than the corresponding strain in a graphene sheet in that particular configuration. The lower critical strain in CNTs is attributed to its curvature, which allows a better relaxation of energy. The reduction in critical strain for a CNT and graphene sheet in a zigzag configuration is more (13.61–14.28) than that for an armchair configuration (6.24–6.50). This is consistent with the results in the literature,[6] where the corresponding strains are (12.5–10.50) and (7.0–6.0).

V. SUMMARY

The atomistic simulations provide profound insights into the microscopic mechanics of defects under applied strain. However, computational expense often precludes the extension of atomistic simulations to very large systems. Continuum formulation presented in this article gives a clear mechanistic interpretation of this phenomenon. We have presented closed-form and semiclosed-form expressions to compute the critical strain for defect nucleation, both in the framework of continuum elasticity theory as well as the gauge field theory. Application of classical formulation to study the nucleation of the SW defects is hindered by the fact that the stresses and strains from the classical solution are singular at the center of nucleation, although classical solu-

tion results are reasonably good. The gauge theory formulation used in this study is free from such singularity of stresses and strains at the center of nucleation. Results from the gauge theory presented in this study are close, both qualitatively and quantitatively, to the existing atomistic simulations. One of our conclusions is that by incorporating the relevant physics, continuum formulation can be a powerful tool for exploring nanoscale phenomena in CNTs.

ACKNOWLEDGMENTS

The authors wish to acknowledge the support of the Texas Institute for the Intelligent Bio-Nano Materials and Structure for Aerospace Vehicles, funded by NASA Cooperative Agreement No. NCC-1-02038. One of the authors (P. S.) is appreciative of the encouragement and support from David Zimmerman and Dimitris Lagoudas.

[1]M. S. Dresselhaus, G. Dresselhaus, and P. C. Eklund, *Science of Fullerenes and Carbon Nanotubes* (Academic, New York, 1996).
[2]M. B. Nardelli, B. I. Yakobson, and J. Bernholc, Phys. Rev. Lett. **81**, 4656 (1998).
[3]I. Ponomareva, L. A. Chernozatonskii, A. N. Andriotis, and A. Menon, *Carbon Nanotube-Junction Structural Properties and Device Applications* (poster) (TNT, 2003).
[4]B. I. Yakobson, C. J. Brabec, and J. Bernholc, Phys. Rev. Lett. **76**, 2511 (1996).
[5]M. B. Nardelli, B. I. Yakobson, and J. Bernholc, Phys. Rev. B **57**, R4277 (1998).
[6]Q. Zhao, M. B. Nardelli, and J. Bernholc, Phys. Rev. B **65**, 144105 (2002).
[7]P. Zhang, P. E. Lammert, and V. H. Crespi, Phys. Rev. Lett. **81**, 5346 (1998).
[8]C. J. Brabec, A. Maiti, and J. Bernholc, Chem. Phys. Lett. **219**, 473 (1994).
[9]L. G. Zhou and S. Q. Shi, Appl. Phys. Lett. **83**, 1222 (2003).
[10]O. C. Zienkiewicz and Y. K. Cheung, *The Finite Element Method in Structural and Continuum Mechanics* (McGraw–Hill, New York, 1967).
[11]David R. Nelson, Phys. Rev. B **26**, 269 (1982).
[12]B. I. Yakobson, Appl. Phys. Lett. **72**, 918 (1998).
[13]B. I. Yakobson, *Proceedings of the Electrochemical Society, Fullerene Symp.*, (1997), Vol. 5, p. 549.
[14]J. P. Hirth and J. Lothe, *Theory of Dislocations* (Wiley, New York, 1982).
[15]A. C. Eringen, Int. J. Eng. Sci. **15**, 177 (1977).
[16]A. C. Eringen, J. Appl. Phys. **54**, 4703 (1983).
[17]B. S. Altan and E. C. Aifantis, J. Mech. Behav. Mater. **5**, 355 (1994).
[18]B. S. Altan and E. C. Aifantis, J. Mech. Behav. Mater. **8**, 231 (1997).
[19]A. Kunin, *Theory of Elastic Media with Microstructure* (Springer, Berlin, 1986).
[20]M. C. Valsakumar and D. Sahoo, Bull. Mater. Sci. **10**, 3 (1988).
[21]M. Lazar, Ann. Phys. **11**, 635 (2002).
[22]M. C. Valsakumar and D. Sahoo, Phys. Lett. A **215**, 305 (1996).
[23]L. D. Landau and E. M. Lifshitz, *Theory of Elasticity* (Addison–Wesley, Reading, MA, 1970).
[24]J. Tersoff, Phys. Rev. B **46**, 15546 (1992).
[25]P. Lenz and D. R. Nelson, Phys. Rev. E **67**, 031502 (2003).
[26]O. L. Blakslee, D. G. Proctor, E. J. Seldin, G. B. Spence, and T. Weng, J. Appl. Phys. **41**, 3373 (1970).
[27]B. S. Altan and E. C. Aifantis, Scr. Metall. Mater. **26**, 319 (1992).